https://doi.org/10.15407/ufm.24.01.106

M.O. VASYLYEV [1,*] and P.O. GURIN [2]

[1] G.V. Kurdyumov Institute for Metal Physics of the N.A.S. of Ukraine,
36 Academician Vernadsky Blvd.,
UA-03142 Kyiv, Ukraine

[2] P.L. Shupyk National Healthcare University of Ukraine,
9 Dorogozhytska Str.,
UA-04112 Kyiv, Ukraine

* vasil@imp.kiev.ua, vasil1934@ukr.net

STRUCTURE AND PROPERTIES OF 3*D* PRINTED ZIRCONIA APPLIED IN DENTISTRY

During the last years, the interest in the application of the additive manufacturing (AM), also known as 3*D* printing, becomes extremely popular in the various fields of the medicine including the dentistry. Currently, metal and ceramic materials are most often used for dental prosthetics manufactured by 3*D* printing. The yttria-stabilized zirconia (YSZ) ceramics has become the best alternative for metal-based dental restorations. In this regard, the main goal of this review deals with studying the effect of the 3*D* printing parameters on the macro- and microstructure and, accordingly, on the mechanical properties of the sintered YSZ, and on this basis, to give the practical recommendations to clinical dentistry and further prospects. As most researched in recent years, the 3*D* printing methods of such ceramics are the Laser-Stereolithography (Laser-SL) and the Stereolithography-Digital Light Processing (SL-DLP) based on the vat-photopolymerization technology and are discussed here. The physical foundations and the technological parameters of these AM technologies are considered. The main attention focuses on the effects of the thermal conditions during the 3*D* printing on the solidification microstructure (density, grain size, and crystalline phase composition), which is controlled by the manufacturing technologies. In addition, the true hardness and the biaxial flexural strength of the 3*D* printed YSZ samples are discussed. At last, the advantages of 3*D* printing ceramics in dentistry are mentioned.

Keywords: dentistry, additive manufacturing, 3*D* printing, zirconia, microstructure, hardness, flexural strength.

Citation: M.O. Vasylyev and P.O. Gurin, Structure and Properties of 3*D* Printed Zirconia Applied in Dentistry, *Progress in Physics of Metals*, **24**, No. 1: 106–131 (2023)

1. Introduction

Over the last decade, the 3*D* printing already has been used in the numerous medical sectors, including biocompatible scaffolds, human osteosarcoma, blood vessels, cartilage, hip joints, knee joints, bones, and soft tissues, as well as dental industry [1–5]. Integration of the various 3*D* printing technologies into different directions of the modern dentistry has attracted the worldwide interest of the research groups. In particular, this technology has been successfully used for the manufacturing of the dental constructions, such as dental implants, crowns, bridges and prosthetic parts with complex geometry using various types of the metals [6–10] and ceramics as initial materials [1, 12].

Zirconium Oxide for Medical Purposes. The high mechanical properties (*e.g.*, the compression strength of about 2000 MPa, the bending strength of 900–1200 MPa, and the fracture toughness of 5–10 MPa $\cdot$ m$^{1/2}$) promote widespread use for the numerous areas in the engineering, for example, to cutting tools, resistive heating elements and oxygen sensors, thread guide, cams, seals, valves, aerospace, and pump impellers with excellent performance [13]. Thanks to its extra aesthetic characteristics and biocompatibility, zirconia has also been very popular in biomedical applications such as surgical implants. The first proposal to use the zirconium oxide for medical purposes was made in 1969 and concerned orthopaedic application. ZrO_2 was proposed as a new material for hip head replacement instead of titanium or alumina prostheses [14, 15].

In recent years, zirconia-based ceramics have become increasingly popular and have generated considerable interest in the dental community because of their biocompatibility, low bacterial adhesion, enhanced aesthetics, and match to traditional cementation procedures as well as excellent mechanical properties [16–20]. This popularity from the superiority of zirconia over the counterparts made of the traditional titanium or CoCr alloys used for the dental applications (prostheses, crowns, bridges, implants, veneers and other). For these applications, zirconia is stabilized at room temperature with the addition of 3 mol.% yttria. These configurations reach high strength (800–1200 MPa) good fracture toughness (6–15 MPa $\cdot$ m$^{1/2}$) and have been successfully adopted at clinics.

Zirconia Crystallographic Structures. As is known, at the ambient pressure, unalloyed zirconia (ZrO_2) is polymorphic and forms the three distinct crystallographic structures depending on the temperature: cubic (fluorite) structure ($Fm3m$) at high temperatures (>2370 °C), tetragonal structure ($P4_2/nmc$) at intermediate temperatures (1200 °C –2370 °C), and monoclinic symmetry ($P2_1/c$) at low temperatures (<950 °C) (Fig. 1). The transformation from the tetragonal (t) phase to the monoclinic (m) phase upon cooling is accompanied by a substantial increase in volume (≈4.5%), sufficient to lead to catastrophic failure. This transformation

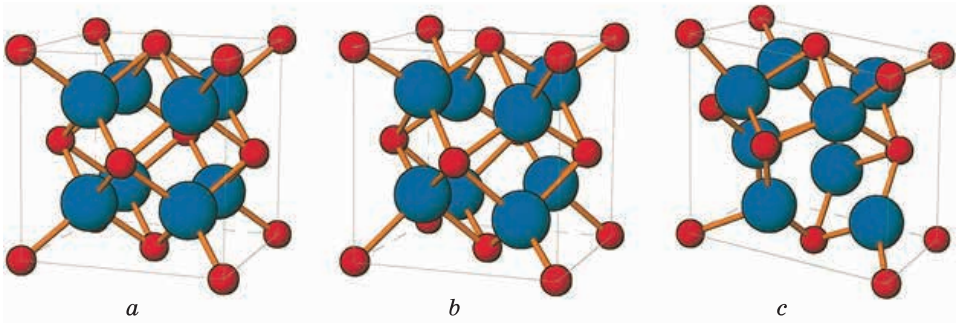

Fig. 1. Schematic representation of the pure ZrO_2 structures: monoclinic (*a*), tetragonal (*b*), and cubic zirconia (*c*) [23, 25]

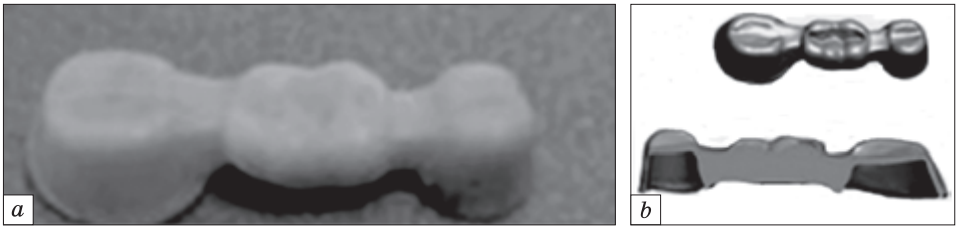

Fig. 2. The CAD/CAM dental bridge (*a*) and its corresponding three-dimensional model (*b*) [59]

is reversible and begins at ≈950 °C on cooling. For this type of the ceramics, such a phenomenon as transformation toughening was observed and explained as non-diffusion martensitic phase transformations similar to iron alloys. It was first reported in the paper entitled 'Ceramic Steel?' in Refs. [22, 23]. Such phase transformations are reversible, and involve the expansion of the core bulk by approximately 3 to 4%, and consequently, progressive microcracks and surface crumbling [24].

To suppress the crack propagation during the phase transformation induced by internal stress different oxides, such as yttrium oxide (Y_2O_3), calcium oxide (CaO) or magnesium oxide (MgO), are added to zirconia in order to stabilize the tetragonal form at room temperature after sintering. Such stabilizers allow achieving the stable fracture toughness, high tensile strength, high hardness and corrosion resistance [26–28]. The fully stabilized zirconia is obtained by adding sufficient amounts of the stabilizing oxides, such as 16 mol.% MgO, 16 mol.% CaO or 2–3 mol.% Y_2O_3.

CAD/CAM Technique in the Dentistry. Now, two modern techniques are extensively used in the prosthetic dentistry for the fabrication of the zirconia dental parts, namely, the computer-aided design combined with the computer-aided manufacturing (CAD/CAM) and additive manufacturing (AM). In the CAD/CAM technique the small, precise milling tool to create the restoration from the pre-sintered or sin-

tered zirconia block are used [29, 30]. However, disadvantages of the milling include the waste of the raw materials and possible microscopic the surface cracks in the sintered dental device. Furthermore, CAD/CAM processing into complex shapes is difficult and includes limited accuracy [31].

Additive Manufacturing Zirconia in Dentistry. To overcome the limitations of the conventional CAD/CAM manufacturing methods, new techniques are introduced, such as additive manufacturing (AM) also called 3*D* printing techniques, enabling the manufacture of the ceramic parts with complex shapes, high precision, high material utilization, reduced cost and no need for cutting tools and [32–36]. Integration of the various 3*D* printing technologies into different directions of the modern dentistry has attracted the worldwide interest of the research groups. In particular, this technology has been successfully used for the manufacturing of the dental constructions, such as dental implants, crowns, bridges and prosthetic parts with complex geometry using various types of the metals [37–41] and ceramics as initial materials [42].

Presently the zirconia (ZrO_2) dental ceramics has become the best alternative for metal-based dental restorations. This material has been used to fabricate the dental prostheses in the early 1980s and gained considerable attention in the dental community. It is due to its unique properties, in particular, such as excellent aesthetics including tooth-like colour, high fracture toughness, flexural strength, good corrosion resistance, and biocompatibility. In recent years, among the various zirconia-based ceramics for AM technology the most popular is the yttria-stabilized zirconia (YSZ) with the tetragonal structure for different clinical applications. Due to its outstanding material properties, it is used for load-bearing applications, such as dental crowns, bridges, veneers, and implant abutments. YSZ restorations have been used in clinical practice over the past two decades [43–57]. The most researched in recent years 3*D* printing methods of the dental YSZ are the laser-stereolithography (laser-SL) and the stereolithography — digital light processing (SL-DLP)

The physical foundations of the 3*D* printing main methods in the dentistry and the results on the structure and mechanical properties recent studies of the 3*D*-printed YSZ zirconia samples are discussed below.

2. 3*D* Printing Techniques of Dental YSZ Parts

2.1. Laser-SL Process

'Stereolithography', invented by Chuck Hull [58], was one of the first 3*D* fabrication technologies of the solid parts. This technique involves the locally activates the chemical polymerization reaction of the liquid monomers from exposure to ultraviolet radiation by the laser.

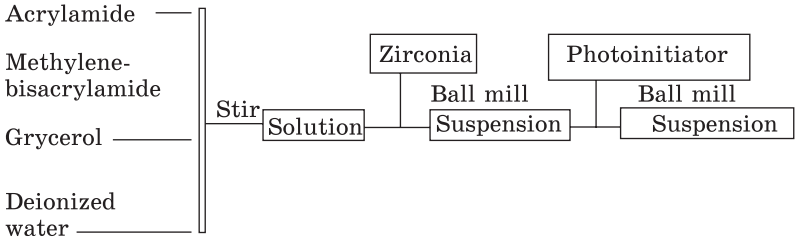

Fig. 3. 3Y-TZP ceramic suspension preparation process [59]

At the first stage of creating the denture by Laser-SL process, there is 3*D* model construction. For example, the 3*D* dental bridge model is obtained by Micro-CT scanning and reverse engineering of the CAD/CAM manufactured dental bridge (Fig. 3, *a*) [59]. The reversed model (Fig. 3, *b*) mainly comprises complex occlusal curves and thin shells (0.5 mm thickness).

Suspension Preparation. The next technological process is the suspension preparation including the 3Y-TZP particles ceramic. The suspension preparation process is illustrated in Fig. 3. Such suspension is the aqueous dispersion of the submicron sized 3Y-TZP particles (mean particle diameter of 0.2 μm). There are three steps of the suspension preparation process. At the step 1, the acrylamide and methylenebisacrylamide are first dissolved in the solution of the deionized water and glycerol. This solution is stirred for half an hour under the ultrasonic dispersion, in order to the solute was fully dissolved. At the step 2, the 3Y-TZP powder is then added incrementally until up to 40 vol.% of the suspension. Every time after this powder was added, the suspension is stirred for ten minutes and then ball milled for one hour. At last, at the step 3, photoinitiator liquid is added and then the suspension is ball milled for half an hour. Received viscosity of ceramic suspension is measured as 127.4 mPa·s by the rotary viscometer.

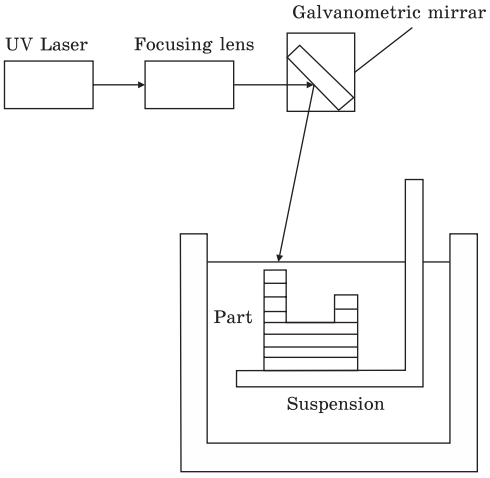

Fig. 4. Scheme of the Laser-SL process [59]

The scheme of the Laser-SL process is presented in Fig. 4. The prepared zirconia ceramic suspension is put to the vat of the 3*D* printer. Then three dimensional model data is converted into the stereolithography file format, and sliced into the series of two dimensional data

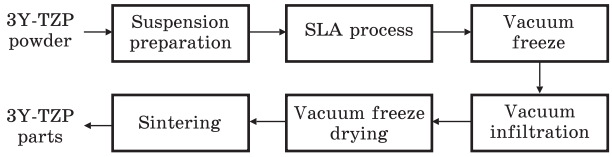

Fig. 5. Laser-SL manufacturing process route [59]

with uniform thickness and the UV laser spot scanned in the certain areas on the ceramic suspension surface, monomers at the irradiated areas are polymerizing upon their exposure to the light. The exposure dose of the radiation must be controlled by adjusting the scanning speed. After one single layer was created, the platform went down and uncured suspension covered up the polymer layer. In this way, so-called, the 'green' ceramic part is manufactured. The overall Laser-SL manufacturing route is illustrated in Fig. 5. The main technical characteristics of the 3*D* printer are as follow: lateral resolution 6–140 μm; printing speed 14 mm/h; maximum print size 27–750 mm.

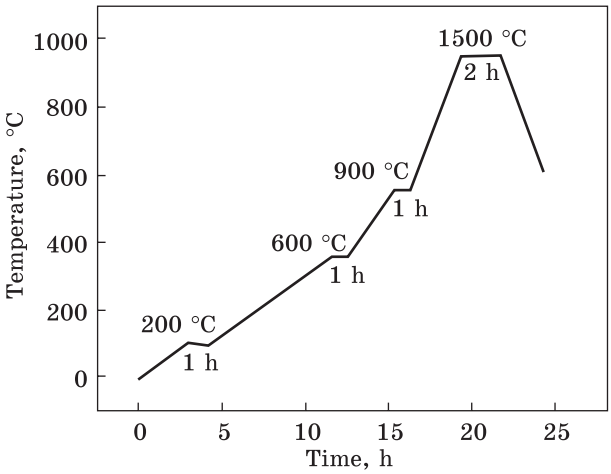

Fig. 6. Sintering temperature program [59]

2.2. Post Laser-SL 3D Printing

After 3*D*-forming processing, the obtained zirconia green parts are then treated by vacuum freeze-drying, vacuum infiltration, and sintering. Vacuum infiltration process was used to increase the density of the green bodies. Infiltration was conducted under 82 kPa using aqueous zirconia ceramic slurry of 40 vol.%. Next step is sintering process, which is performed according to the temperature control protocol shown in Fig. 6.

3. Stereolithography-Digital Light Processing (SL-DLP)

SL-DLP is considered an interesting 3*D* technology in recent years because it is able to print ceramic parts with high quality and fairly fast time because the printing method is done per layer [60–64]. The process of the photochemical reaction and curing in SL-DLP printer is fairly faster than laser-SL printer, since the last uses laser light photopolymer

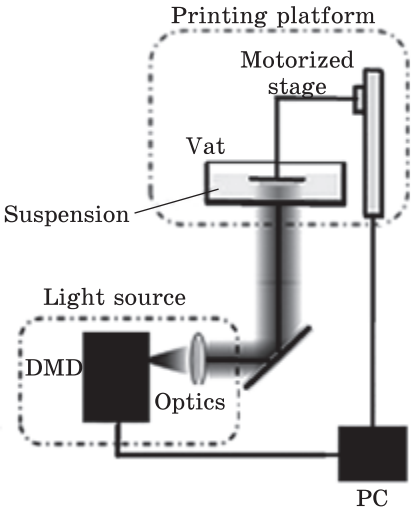

Fig. 7. Scheme of SL-DLP based 3*D* printer [68]

sources that process layer by layer. The SL–DLP technique firstly forms green parts through light curing the resins in ceramic slurry [65]. The SL-DLP is based on the vat-polymerization technology, and is similar to laser-SLA and can be classified into same category but it differs in terms of the light source used. It also uses the characteristics of the photosensitive material to polymerize and solidify under ultraviolet light irradiation [66]. Compared to other 3*D* printing techniques, the SL-DLP technique has advantages in forming small ceramic objects with high accuracy requirements, considered as a preferred technique for 3*D* printing dental zirconia prostheses. The SL-DLP-system creates the ceramic green part by stacking up layers of the photocurable resin with the solid loading of around 45 vol.% zirconia powder. The DLP-system instead of the laser to polymerization of the photosensitive polymers as build material uses the Light Emitting Diodes (LED), **which** is generated by digital mirror device (DMD) [67].

The typical SL-DLP based printer consists of three key components: the light source, the printing platform and the photocurable precursor (suspension) (Fig. 7). SL-DLP based 3*D* printer has the constant parameter light curing strategies (LCS), that allow the operator to choose the light intensity (mW/cm^2) and the exposure time (s) depending on the polymerization characteristics of the suspension. After one layer is completed, the suspension fresh layer is coated and the process is repeated until the so-called green part is built with the typical layer thicknesses range

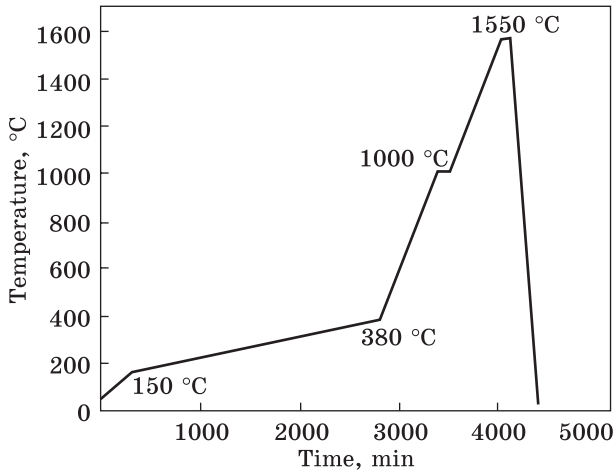

Fig. 8. Thermal debinding and the sintering program [71]

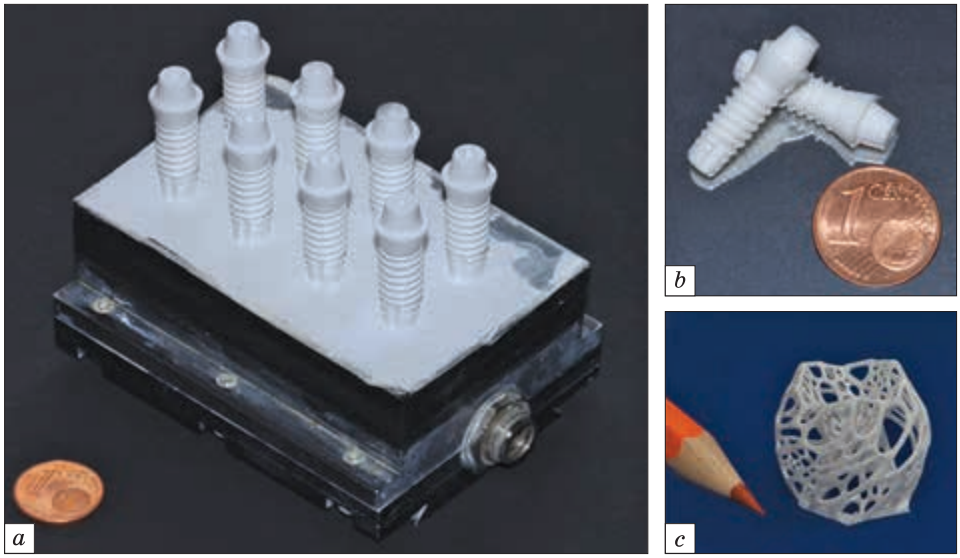

Fig. 9. Green parts (*a*), sintered parts (*b*), and a cellular structure made of ZrO_2 (*c*) fabricated using the SL-DLP-based 3*D* printing [69]

from 15 μm to 100 μm. The digital micro mirror device dynamically generates the images used for light curing. The light source serves as the energy input to activate some reactive species and allow the photochemical reactions (polymerization) to take place. 3*D* printing process parameters are one of the process variables that can affect the quality of the printed parts [69]. The SL-DLP printing firstly forms the green parts through light curing the resins in the ceramic suspension (slurry). In particularly, the zirconia slurry for printing are composed of 78 wt.% Y-TZP powder and photosensitive resin (2-hydroxyethyl) of 2 wt.% [70]. After printing, the parts are soaked in deionized water at approx. 40 °C for 24 h to remove uncured slurry. Then, these are oven dried at 70 °C for 6 h and finally submitted to the thermal debinding and sintering, depicted in Fig. 8. In particular, samples were slowly heated up to 1000 °C to avoid cracking during resin decomposition and then sintered up to 1550 °C (heating rate 1 °C/min) for 1 h in order to achieve the dense ceramic part (Fig. 9).

4. Characteristics of 3*D*-Printed YSZ Samples

4.1. Laser-SL Techniques

Ref. [72] (2018). After laser-SL forming processing, the obtained zirconia green bodies were then treated by vacuum freeze-drying, vacuum infiltration, and sintering. The zirconia 3*D*-samples densities depending on the post processes were determined by Archimedes method. Apparent

porosity and solid density were recorded and presented in Table 1. In addition, one can see here the relative density, which was calculated to comparison. From the Table 1 it is clear that apparent porosity rate of the green body was 23.46%; and after sintering, the apparent porosity of the zirconia 3*D*-samples decreased and the solid density increased significantly. Surface roughness of the sintered 3Y-TZP zirconia 3*D*-dental bridge was measured and compared to the CAD/CAM dental one. In term of the occlusal curve surface roughness, the CAD/CAM dental bridge is obviously smoother than laser-SL dental bridge (1.57 μm *vs.* 2.06 μm). However, as thin shells, the CAD/CAM dental bridge is rougher than light cured dental bridge (2.43 μm *vs.* 2.23 μm).

Mechanical Properties. The Vickers hardness of the zirconia ceramic bridges were tested as 1398 *HV*, which is much better than by CAD/CAM processes (1185 *HV*). The zirconia ceramic parts without infiltration had a three-point bending strength of 168.7 MPa. Lase-SL fabricated dental bridge with the three-point bending flexural strength of 200.14 MPa is not good enough for the actual clinical dental practical. The reason for this is explained by the formation the internal defects (Fig. 10) which formed by the laser-SL process. Mechanical strength of zirconia parts is affected by its density and microstructure. Therefore, to solve this problem, the optimal laser-SL process and the sintering process need further research.

Table 1. **Densities of zirconia 3*D*-samples [72]**

Stage	Apparent porosity, %	Apparent solid density, $g \cdot cm^{-3}$	Relative density, %
Green body	23.46 ± 1.05	2.65 ± 0.05	—
Sintered without infiltration	7.84 ± 1.03	5.79 ± 0.19	94.84%
Sintered with infiltration	0.75 ± 0.46	6.03 ± 0.10	98.58%

Table 2. **Mechanical properties of the 3*D*-printed samples [73]**

Samples	Flexural strength, MPa	Vickers hardness, *HV*
Horizontal direction *H*	499	1363
Vertical direction *V*	576	1398
Control	1143	1402

Table 3. **Relative amounts of each phase for the 3Y-TZPs [74]**

Type of the manufacture	*t*-ZrO_2, wt.%	*c*-ZrO_2, wt.%	*m*-ZrO_2, wt.%
3*D* printing	86.4	13.4	0.1
Subtractive manufacture	87.6	12.2	0.2

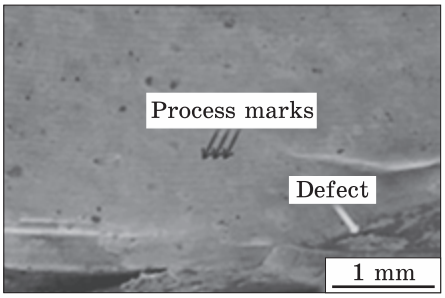

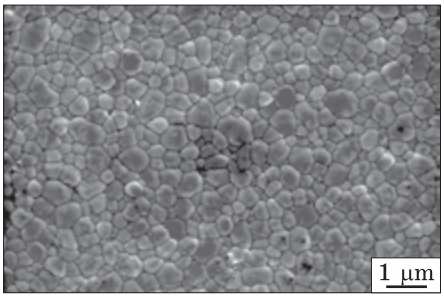

Fig. 10. Macroscopic structure of the zirconia 3*D*-parts [72]

Fig. 11. SEM micrograph of the zirconia printed sample after sintering at 1500 °C [73]

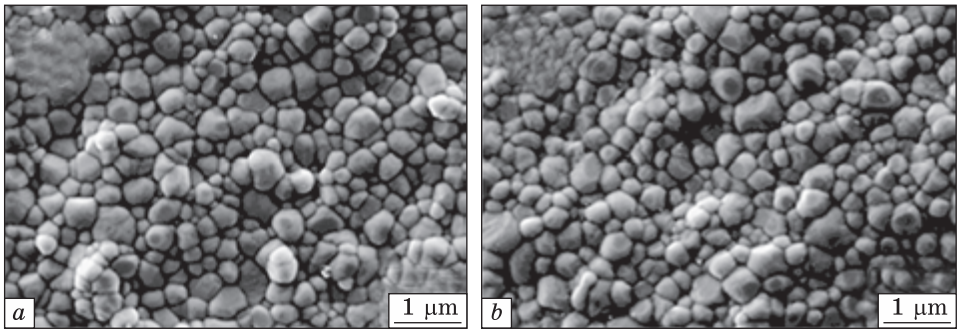

Fig. 12. Representative SEM photomicrographs: *a* — subtractively manufactured 3Y-TZP; *b* — 3*D*-printed 3Y-TZP [74]

Ref. [73] (2019). After 3*D* printing, the zirconia samples were carbon-debinded and sintered under the following conditions: debinding time 81.9 h with maximum temperature 500 °C, and sintering time 48.9 h with maximum temperature 1500 °C. Optical microscopy and scanning electron microscopy (SEM) revealed that the samples were randomly delaminated between the printing layers. At the same time, the printed layer thickness varied from 13 μm to over 20 μm. Microstructure examinations indicated that the average grain size after sintering is 392 nm for the printed samples (Fig. 11).

Mechanical properties. The flexural strength and Vickers hardness were determined for the samples 3*D*-printed in vertical (*V*) or horizontal (*H*) orientation. As control group, the milled samples were used. The results are shown in Table 2. As seen in Table 2, the achieved average 3-point flexural strengths for sample 3*D*-printed in horizontal orientation and sample 3*D*-printed in the vertical orientation are low compared to the control group.

Ref. [74] (2021). Here, the microstructures of the 3*D*-printed and subtractive manufactured zirconia (3Y-TZP) samples were compa-

red. The x-ray diffraction (XRD) analysis revealed that both types of the samples contained t-ZrO_2 phase, c-ZrO_2, and m-ZrO_2, which are typical for 3Y-TZP ceramics (Table 3). The representative SEM image of the 3*D*-printed 3Y-TZP sample is presented in Fig. 12. Thus, the complex analysis revealed the comparable phase composition and microstructure for the additively manufactured 3Y-TZPs and subtractively manufactured ones. However, the microstructural analysis revealed that pores were more frequently detected in the subtractively manufactured zirconia.

Mechanical properties. Regarding biaxial flexural strength, significant differences were observed between subtractively manufactured 3Y-TZP and additively manufactured one. The 3*D*-printed sample had higher biaxial flexural strength (1108.9 MPa) than additively and subtractively manufactured 3Y-TZP (934.8 MPa).

4.2. SL-DLP Techniques

Ref. [75] (2017). The custom dental implant was designed and 3*D*-printed using the zirconia Y-TZP powder (Y_2O_3 5.2 wt.%) by the SL-DLP. The digital file of the designed custom implant and the 3*D*-printed implant are presented in Fig. 13. The sintering process with the maximum temperature of 1500 °C to obtain fully densified specimens (average, 99.9%) was performed. According to SEM analysis the micro-porosities of the representative intact samples ranged in the size from 196 nm to 3.3 μm. Quantitative measurement of the surface roughness showed the mean R_a value of 1.59 μm and R_q value of 1.94 μm. As expected from x-ray analysis, the 3*D*-printed implant showed the standard pattern for sintered Y-TZP zirconia.

Mechanical properties. The biaxial flexure strength test was evaluated using for the samples, which were 3*D*-printed in the three different printing angles: 0° (vertical), 45° (oblique) and 90° (Horizontal). It was obtained that the 3*D*-printed samples exhibited the high flexure strength value (943 MPa) comparable to that of milled zirconia (800 MPa). The 0-degree, vertical build orientation resulted in the highest flexure strength values, whereas the lowest values were observed with 45 degrees printing angle. This may be due to the difficulty in attachment of the subsequent layers of the disc shape for 45° build angle resulting in more structural defects of the printed object.

Ref. [76] (2019). In this work, 3*D* manufacturing was applied to fabricate the dental bridges and implants made of zirconia. In these experiments, multiple acrylates and methacrylates were used as monomers, and 3 mol.% yttria-stabilised zirconia (3Y-TZP) powders, together with suitable photoinitiator, dispersant agent and other additives, are added to monomers to obtain homogenous hybrid suspension that can be photocured by the SL-DLP 3*D* printer. After 3*D* printing, the

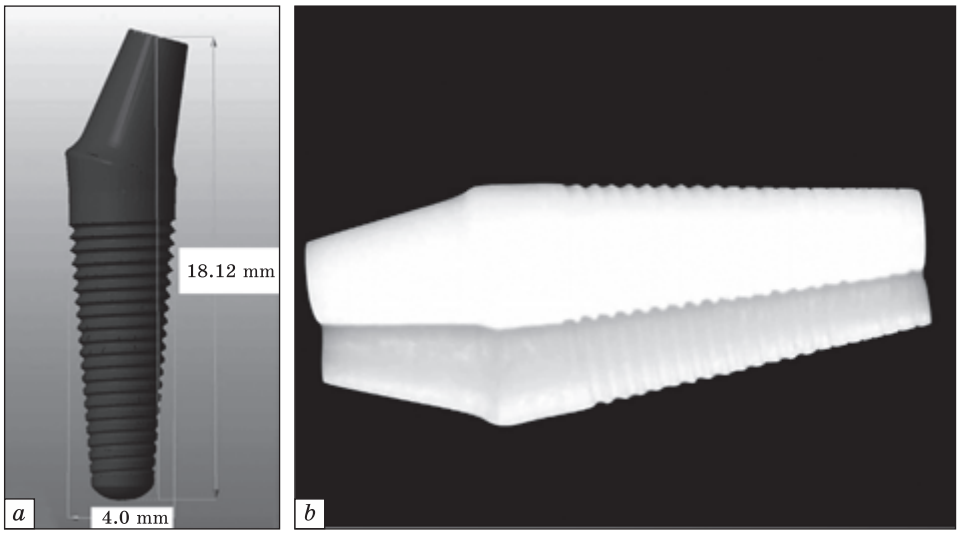

Fig. 13. 3*D*-CAD design of the dental implant (*a*), and 3*D*-printed zirconia implant (*b*) [75]

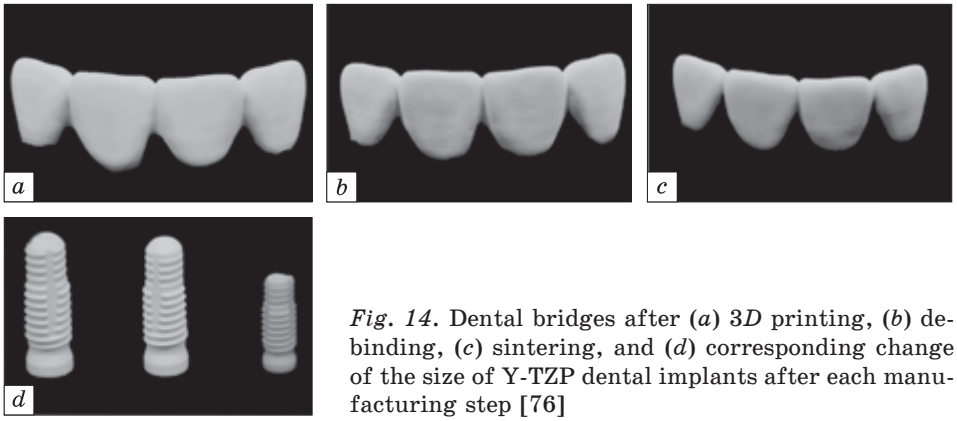

Fig. 14. Dental bridges after (*a*) 3*D* printing, (*b*) debinding, (*c*) sintering, and (*d*) corresponding change of the size of Y-TZP dental implants after each manufacturing step [76]

debinding process was performed by slowly heating up to 523 °C for complete organics removal, and further pre-sintering at 800 °C with a soaking time of 1 h. The final sintering process was conducted with the maximum sintering temperature of 1450 °C in air.

Such structural features, as particle packing, grain growth and interlayer coherence evolution during the sintering process, were characterized in this studied. Figure 14, *a* shows the photo of the 3*D*-printed hybrid green body. Sufficient debinding and sintering procedure should be provided for obtaining dense parts. It was observed that the precision of the final dental parts mostly depends on the homogeneity of the hybrid suspension, the layer thickness along the *Z*-axis, the resolution of

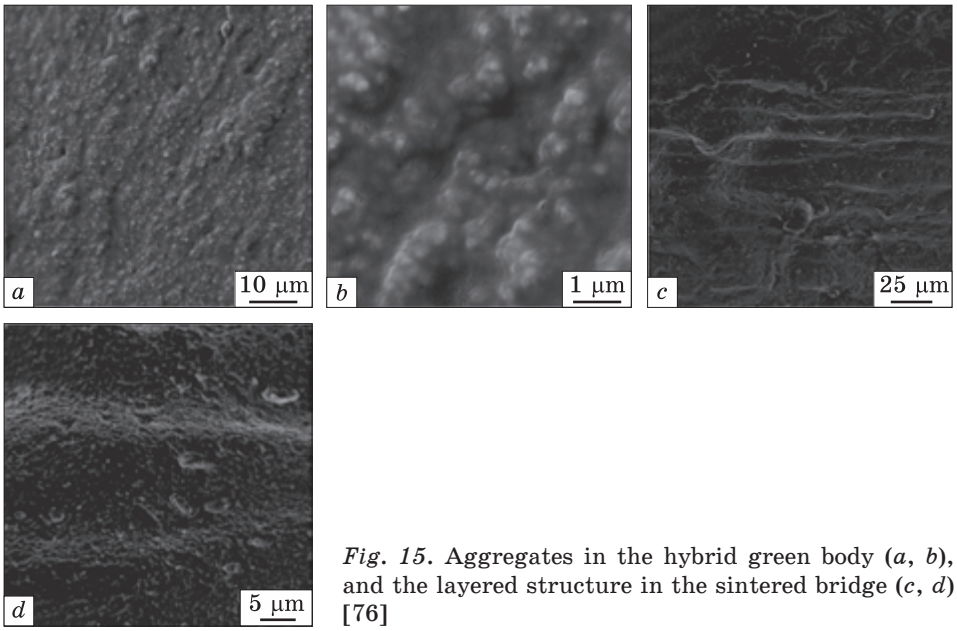

Fig. 15. Aggregates in the hybrid green body (*a*, *b*), and the layered structure in the sintered bridge (*c*, *d*) [76]

light exposure on the X–Y plane, and the shrinkage during curing and densification in the debinding-sintering process. In the case of the presented work, those aggregates have similar size of the several microns (Fig. 3, *a*, *b*) which would lead to further inhomogeneity in the printed layered structures as follows. For possible to dental application in the surface precision of about 20 μm is required to ensure marginal fit, so the smaller layer thickness, like 25 μm, is preferred in SL-DLP stereolithography for the high marginal precision in the dental practice. Obviously, this value is close to the size of the observed aggregates on scale, so local aggregates would severely deteriorate the smoothness for the 3*D*-printed layer. It is often leading to the wavy surface and layered structures after photocuring and the sintering processes (Fig. 15, *c*, *d*).

Ref. [77] (2019). The aim of the present study was to show the influence of the zirconia volume fraction in the suspension on the microstructure samples printed by SL-DLP. The zirconia suspensions were mixed with 3 mol.% Y_2O_3 stabilized zirconia powder, acrylates and dispersant. Specimens were divided into six groups based on zirconia volume fraction in the range of 48–58 vol.%. All organic binders were removed at 600 °C under air atmosphere. The final sintering step was performed at 1450 °C. XRD analysis showed the diffraction peaks of 2θ at 30.2°, 34.7°, and 35.2° corresponding to characteristic of the tetragonal planes (101)*t*, (002)*t*, and (110)*t* of *t*-ZrO_2, respectively. The amount of *m*-ZrO_2 was below the detection limit in all specimens. In the cross of green bodies of all groups, the repeated layers with thickness of 25 μm

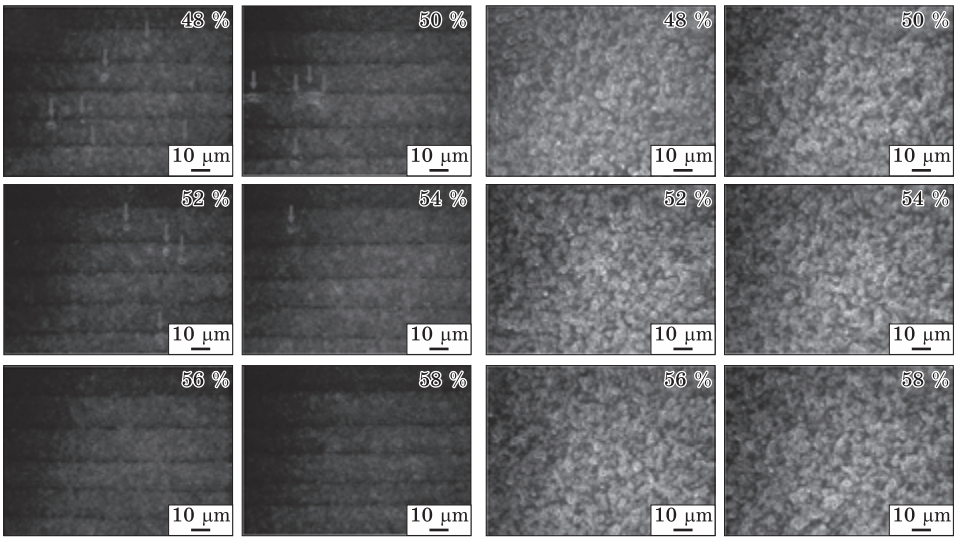

Fig. 16. Cross-sectional SEM images for the different volume fractions of zirconia: *a* — green body samples (the arrows show defects that appeared when the zirconia volume fraction decreased); *b* — sintered samples [77]

were observed. It was also noted that the defects (marked with arrows in Fig. 16, *a*) increased in number when the zirconia volume fraction decreased. However, after sintering processes, such repeated layers and defects were no longer visible (Fig. 16, *b*).

Mechanical properties. The influence of the zirconia suspensions composition on the mechanical test was studied. It was established that the 3-point bending strength of the 3*D*-printed samples increased as the volume fraction of the zirconia powder in the suspension increased, reaching a maximum value of 674.74 MPa for the volume fraction of 58 vol.%. Whereas for minimum fraction (48 vol.%) the bending strength ranged from was 94 MPa.

Ref. [78] (2021). The purpose of the study was to determine the hardness and fracture toughness of dental yttria-stabilized tetragonal zirconia polycrystal (Y-TZP) manufactured SL-DLP technology and Mill as the control samples to study its clinical prospects. The zirconia suspension for printing was composed of 58 vol.% Y-TZP powder and photocurable monomers. Firstly, the green parts of the DLP group were printed layer by layer under a light intensity of 90 mW/cm^2 with 25 μm each layer. Then, the debinding process was performed by putting the green parts into the debinding furnace under 100–450 °C to remove organic parts. At last, the final sintering process was carried out on Y-TZP of the two groups by sintering them for 2 h at 1510 °C with heating and cooling rates set at 300 °C/h.

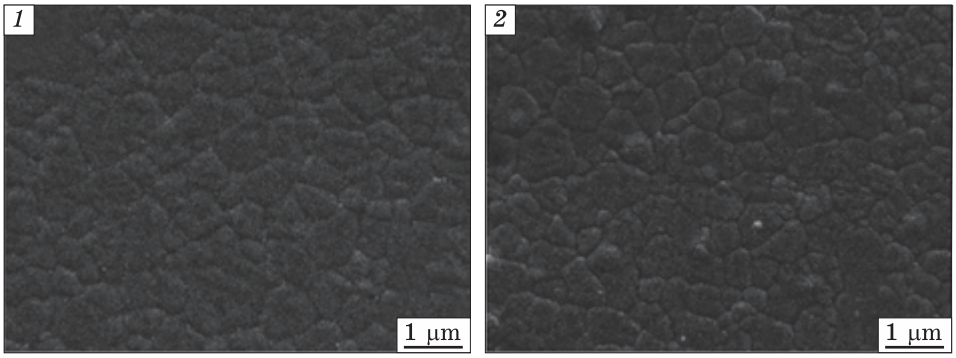

Fig. 17. SEM images of the zirconia surface, where *1* — SL-DLP, and *2* — MILL [78]

As is shown in Table 4, there was no statistical difference between the two groups in density and grain size. The grains of both groups were of tight arrangement with uniform size (see Fig. 17). The XRD pattern shows that only the tetragonal phase was found in the two groups of the zirconia samples. Therefore, the SL-DLP manufactured zirconia parts is similar to milled zirconia one in the microstructure (including density, grain size, and crystalline phase composition).

Mechanical properties. The purpose of this study was to determine the hardness and fracture toughness of the dental yttria-stabilized tetragonal zirconia polycrystal (Y-TZP) manufactured by SL-DLP technology to study its clinical prospects. The results showed that the Vickers hardness of the 3*D*-printed samples (1189 *HV*) is lower than of the conventional milling process (1248 *HV*), which is due to large pores on the surface of the SL-DLP zirconia samples. There is no statistical difference in fracture toughness between SL-DLP-manufactured zirconia (3.43 ± 0.29 MPa$\cdot$m$^{1/2}$) and milled samples (3.44 ± 0.23 MPa$\cdot$m$^{1/2}$), which

Table 4. **Microstructural characterization [78]**

Samples	Density, g/cm^3	Relative density, %	Grain size, μm	Crystalline phase structure
SL-DLP	6.0198	99.0099	0.6030	Tetragonal
MILL	6.0382	99.3125	0.5911	Tetragonal

Table 5. **The mechanical properties 3*D*-printed samples in the two different directions [79]**

Suspension composition	σ, MPa (*XY*)	*E*, GPa (*XY*)	σ, MPa (*XZ*)	*E*, GPa (*XZ*)	Vickers hardness, *HV* (*XY*)	Vickers hardness, *HV* (*XZ*)
79 wt.%	594	161	706	164	12.35	12.34
81 wt.%	675	166	751	162	12.34	12.00

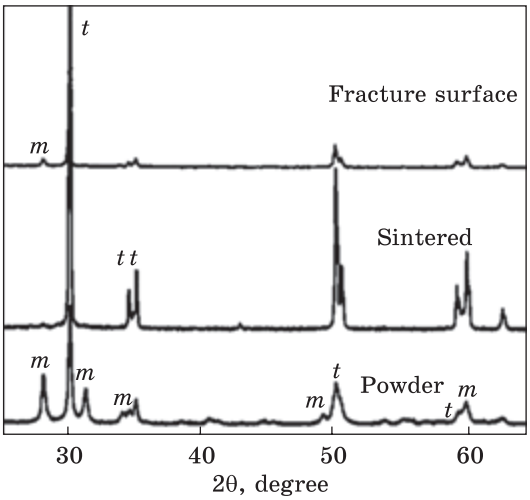

Fig. 18. XRD patterns corresponding to CY3Z powder; 81 wt.% sample sintered 1 h at 1550 °C, and fracture surface of the 81 wt.% sample sintered 1 h at 1550 °C [79]

can be explained by the highly similar microstructure of the both groups samples.

Ref. [79] (2022). In this study, the suspensions were prepared by mixing suitable amounts of the zirconia (CY3Z) powder with a commercial photocurable resin. The suspensions at two different solid compositions were prepared (79 wt.% and 81 wt.%, which correspond to 40.5 vol.% and 43.6 vol.%, respectively), using in both cases 1 wt.% of dispersant respect to the zirconia powder. The crystalline phases presented in the zirconia powder and sintered 3*D*-samples were identified using XRD analysis. These diffraction reflections are shown in Fig. 18. All the patterns present the characteristic peaks of the monoclinic (*m*) and/or tetragonal (*t*) zirconia. It can be noted that the *m*-phase content in the as obtained powder is 48% while no such zirconia is detected in the sintered sample where only the *t*-phase is completely observed.

Figure 19 presents the SEM images of the sintered 3*D*-sample (still at 79 wt.% powder loading) microstructure after polishing and thermal etching. It can see that the low-magnification image of the polished sample (Fig. 9, *a*) shows the high homogeneous and defect-free microstructure, attesting the favourable choice of the suspension properties and 3*D* printing parameters. Higher magnifications images (Fig. 9, *b*, *c*) demonstrate the typical fine-grained microstructure of the yttria-stabilized zirconia, and highlight the fully densified microstructure. As result the fully dense microstructure observed, validate the very high relative density obtained (99.2%). At last, the highest magnification micrograph (Fig. 9, *d*) demonstrates the quite wide dimensional range of the zirconia ceramic grains, as some ultra-fine grains (in the nanometric range) are visible among submicrometric ones. The zirconia grains fall within a certain dimensional range with the majority of the grains in the range 0.40–0.60 μm. In particular, the average grain size for 81 wt.% composition was 0.55 ± 0.19 μm while for 79 wt.% composition was 0.57 ± 0.19 μm.

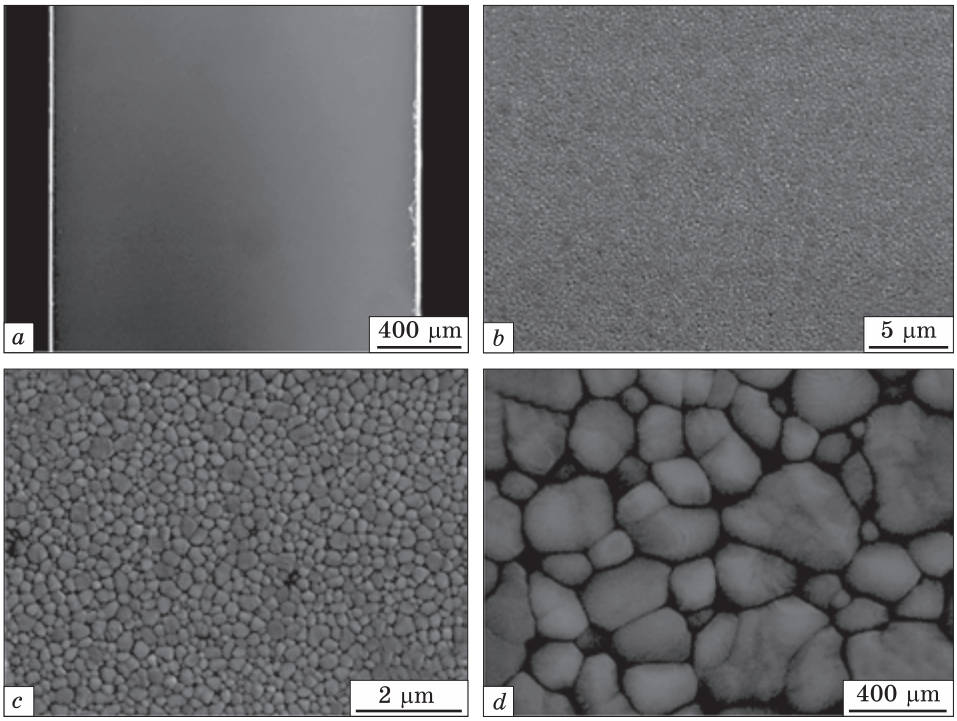

Fig. 19. SEM images with different magnifications of the polished 3*D*-printed sample (79 wt.% zirconia composition) [79]

Mechanical properties. Flexural strength (σ) and Young modulus (*E*) for the perpendicular and parallel 3*D* printing orientation (*XY*, *XZ*) were measured using three-point bending test and the results are reported in Table 5. As seen, the mechanical properties were just slightly influenced by printing direction and zirconia powder composition vol.%. Indeed, the composition with the higher solid composition (*i.e.*, 81 vol.%) had the highest three-point flexural strength when tested perpendicular to the 3*D* printing orientation. On the other side, Young modulus and Vickers hardness are not dependent on the 3*D* printing orientation, and showed values comparable to those of samples manufactured by conventional technologies.

Ref. [80] (2022). The objective of this study is to examine the physical-mechanical and surface properties of 3*D*-printed zirconia (3Y-TZP) in comparison to milled samples. The 3*D*-samples were printed in the horizontal (0°), tilted (45°) and vertical (90°) direction. The milled samples were immediate sintering at 1500 °C. The 3*D*-samples were debinded at 1000 °C, sintered at 1450 °C and then polished. The main tested properties for different samples group are summarized in Table 6.

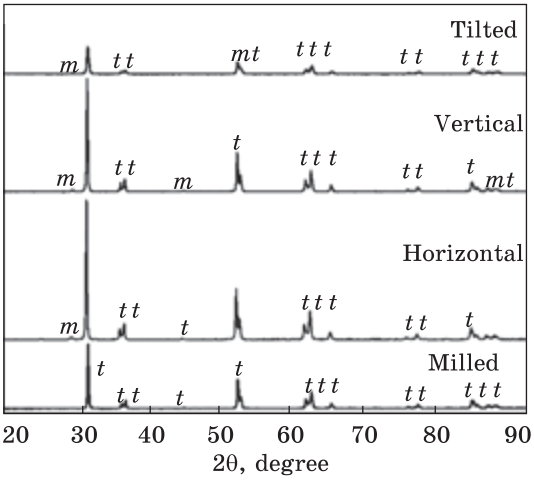

Fig. 20. The XRD pattern of representative specimens from each samples' group [80]

According to the XRD analysis (Fig. 20), the tetragonal phase (*t*) was the principal phase detected for the all groups, with varying percentages of the monoclinic (*m*) structure. In the milled samples, the monoclinic phase compared to 3*D*-printed groups was not observed. The samples had with 0.93, 2.95, and 14.2% of the *m* phase in the horizontal, vertical, and tilted, respectively. For the all samples groups the average grain size ranged between 418 and 458 nm. Concerning crystalline size at maximum diffraction peak intensity, the milled, horizontal, and vertical groups had nearly double the crystalline size of the titled group (Table 6). The highest and lowest densities were reported with milled (6.056 ± 0.116 g/cm^3) and tilted (5.942 ± 0.266 g/cm^3), respectively. The apparent porosity of the specimens ranged between 0.923 ± 0.591% and 1.945 ± 1.509% for milled and tilted with no significant difference between the groups. The highest and lowest surface roughness values were observed for the tilted and milled samples, respectively. As can see in Table 2 the surface roughness of the samples varied significantly: the tilted group had the highest R_a (0.688 μm), significantly different from milled (0.542 μm). However, no difference was detected between the milled and the other two printed groups.

The SEM images of the as-manufactured samples from each group are displayed in Fig. 21 at different magnifications. At low magnification (500×), the milled and horizontal specimens show dense and smooth

Table 6. **Tested properties for different group of samples [80]**

Property	Milled group	3*D* printed group		
		Horizontal	Vertical	Tilted
Density, g/cm^3	6.065	5.978	5.987	5.942
Apparent porosity, %	0.923	0.948	0.970	1.945
Average grain size (measured from SEM), nm	448	420	458	418
Crystalline size (measured from XRD), nm	96	96	96	57
Roughness, μm	0.542	0.626	0.660	0.688

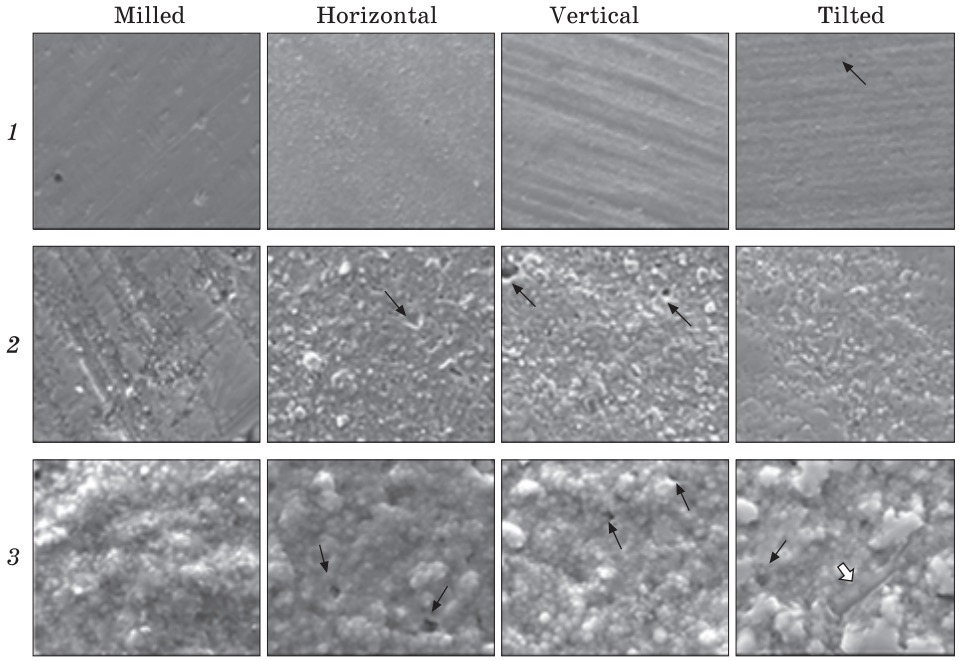

Fig. 21. Surface characteristics of representative samples from each group for different scales (zooming): *1* — 500×; *2* — 5 000×; *3* — 20 000× [80]

surfaces with some irregularities, while, for the vertical and tilted samples, the surface shows clearly bands of the parallel waves of zirconia representing the layers of the 3*D* printing. The higher magnification (5 000×) of the 3*D*-printed samples showed the clustering of the zirconia grains into clumps in addition to the presence of few voids on the surface that ranged between 2 and 10 μm across. After further magnification (20 000×), the milled specimens showed the dense structure with no voids and slightly polygonal grains in the range of 270–760 nm and an average of 450 nm. Smaller voids are detected in printed specimens with rounded grains in the range of 240–920 nm. In addition, the tilted specimen shows deep and wide grooves, as marked by a hollow black arrow with a slight fusion of smaller grains into larger clumps. Voids are marked with black solid arrows.

Table 7. **Mechanical properties of the 3*D*-printed and milled samples [80]**

Samples	Biaxial flexural strength, MPa	Hardness, *HV*
3*D*-printed (horizontal)	1186.73	1676.61
3*D*-printed (vertical)	524.51	1609.54
3*D*-printed (tilted)	810.92	1634.96
Milled	1507.27	1548.21

Mechanical properties. The values of the main mechanical characteristic are presented in Table 7. Concerning the hardness, all 3*D*-printed samples show the close hardness values with no significant difference. The highest hardness value is observed for horizontal direction (1676.61 *HV*) and the lowest for milled samples (1548.2 *HV*). For the biaxial flexural strength, the milled and vertical samples show the highest and lowest values at 1507.27 MPa and 521.51 MPa, respectively.

5. Conclusions

Integration of the various additive manufacturing (3*D* printing) technologies into the various medical fields including the modern dentistry has attracted the worldwide interest among researchers and practicing medical professionals. One of the most important areas of the dentistry is prosthodontics, which is associated with replacing of the missing tooth/teeth. Particularly, 3*D* printing has been successfully used for the manufacturing of the dental devices, such as implants, crowns, bridges and prosthetic parts with complex geometry. In connection with this, there are many different types of the metal alloys and ceramics to be used in the dentistry as the initial construction material. In recent years, zirconia-based ceramics (ZrO_2) have considerable interest in the dental restorations. This is explained by their biocompatibility, low bacterial adhesion, enhanced aesthetics, match to traditional cementation procedures as well as excellent mechanical properties, corrosion and wear resistance. Presently the zirconia dental ceramics has become the best alternative for metal-based dental restorations. Now, two modern techniques are extensively used in the prosthetic dentistry for the fabrication of the zirconia dental parts, namely, the Computer-Aided Design combined with the Computer-Aided Manufacturing (CAD/CAM) and 3*D* printing technologies. However, the Computer-Aided milling has several disadvantages include the waste of the raw materials and possible microscopic the surface cracks in the sintered dental device. Furthermore, it is difficult by the CAD/CAM processing to fabricate the complex shapes of the dental devices and there is the limited accuracy. In order to overcome the limitations of the conventional CAD/CAM manufacturing methods, new techniques are introduced, such as 3*D* printing techniques, which provides the manufacture of the ceramic parts with complex shapes, high precision, high material utilization, reducing cost and no need for cutting tools. Among the various zirconia-based ceramics for 3*D* printing, the most popular is the yttria-stabilized zirconia (YSZ) with the tetragonal structure for different clinical applications. YSZ for the dental restorations have been used in clinical practice over the past two decades. In recent years, the most researched in recent years 3*D* printing methods of such ceramics are the laser-ste-

reolithography (Laser-SL) and the stereolithography-digital light processing (SL-DLP). The both technologies are based on vat-photopolymerization technology but it differ in terms of the light source used (the laser beam or ultraviolet light irradiation).

The 3*D*-manufactured YSZ zirconia is similar to milled zirconia in microstructure, including density, grain size, and crystalline phase composition. According to the XRD analysis, the tetragonal phase (*t*) was the principal phase detected for all the experimental groups. The SEM micrographs revealed the fully dense microstructure with the typical fine-grained microstructure of the 3*D*-printed and sintered zirconia samples with the average grains size of 0.56 ± 0.19 μm. The true hardness of 3*D*-printed and sintered zirconia is 5% lower than that of milled zirconia, which may be attributed to the existence of the several pores on the samples surface. Regarding biaxial flexural strength, significant differences were observed between subtractively manufactured (milled) YSZ and additively manufactured ones. The 3*D*-printed samples had higher biaxial flexural strength (1108.9 MPa) than additively and subtractively manufactured 3Y-TZP (934.8 MPa).

REFERENCES

1. Y. Tang, Y. Zhang, Z. Meng, Q. Sun, L. Peng, L. Zhang, W. Lu, W. Liang, G. Chen, and Y. Wei, *Front. Bioeng. Biotechnol.*, **10**: 964651(2022); https://doi.org/10.3389/fbioe.2022.964651
2. K. Torabi, E. Farjood, and S. Hamedani, *J. Dent.*, **16**: 1 (2015); https://doi.org/10.1016/0300-5712(88)90095-4)
3. Abdullah Barazanchi, Kai Chun Li, Basil Al-Amleh, Karl Lyons, and J. Neil Waddell, *J. Prosthodontics*, **26**: 156 (2017); https://doi.org/10.1111/jopr.12510
4. Danial Khorsandi, Amir Fahimipour, Payam Abasiane, Sepehr Sadeghpour Saber, Mahla Seyedi, Sonya Ghanavati, Amir Ahmad, Andrea Amoretti De Stephanis, Fatemeh Taghavinezhaddilami, Anna Leonova, Reza Mohammadinejad, Majid Shabani, Barbara Mazzolai, Virgilio Mattoli, Franklin R. Tay, and Pooyan Makvandi, *Acta Biomaterialia*, **122**: 26 (2021); https://doi.org/10.1016/j.actbio.2020.12.044
5. A. Dawood, B. Marti Marti, V. Sauret-Jackson, and A. Darwood, *Br. Dent. J.*, **219**: 521 (2015); https://doi.org/10.1038/sj.bdj.2015.914
6. T. Koutsoukis, S. Zinelis, G. Eliades, K. Al-Wazzan, M.A. Rifaiy, and Y.S. Al Jabbari, *J. Prosthodont*, **24**: 303 (2015); https://doi.org/10.1111/jopr.12268
7. K.P. Krug, A.W. Knauber, and F.P. Nothdurft, *Clin. Oral Investig.*, **19**: 401 (2015); https://doi.org/10.1007/s00784-014-1233-2
8. M. Revilla-Leyn and M. Özcan, *Curr. Oral Health Rep.*, **4**: 201 (2017); https://doi.org/10.1007/s00784-014-1233-2
9. M.O. Vasylyev, B.M. Mordyuk, S.M. Voloshko, and P.O. Gurin, *Prog. Phys. Met.*, **23**: 337 (2022); https://doi.org/10.15407/ufm.23.02.337

10. E. Dianne Rekow, *Dental Materials*, **36**: 9 (2020); https://doi.org/10.1016/j.dental.2019.08.103
11. T. Chartier, C. Dupas, M. Lasgorceix, J. Brie , E. Champion, N. Delhote, and C. Chaput, *J. Ceram. Sci. Technol.*, **6**: 95 (2015); https://doi.org/10.4416/JCST2014-00040
12. M. Dehurtevent, L. Robberecht, J. C. Hornez, A. Thuault, E. Deveaux, and P. Behin, *Dental Materials*, **33**: 477 (2017).; https://doi.org/10.1016/j.dental.2017.01.018
13. Xiuping Zhang, Xin Wu, and Jing Shi, *Journal of Materials Research and Technology,* **9**: 9029 (2020); https://doi.org/10.1016/j.jmrt.2020.05.131
14. J. Chevalier, *Biomaterials*, **27**: 535 (2006); https://doi.org/10.1016/j.biomaterials.2005.07.034
15. Y. Chen, J. Moussi, J.L. Drury, and J.C. Wataha, *J. Expert. Rev. Med. Dev.*, **13**: 945 (2016); https://doi.org/10.1080/17434440.2016.1230017
16. W. Höland, V. Rheinberger, E. Apel, C. Ritzberger, F. Rothbrust, H. Kappert, F. Krumeich, and R. Nesper, *J. Eur. Ceram. Soc.*, **29**: 1291 (2009); https://doi.org/10.1016/j.jeurceramsoc.2008.08.023
17. A. Dakskobler, P. Jevnikar, C. Oblak, and T. Kosmac, *J. Eur. Ceram. Soc.*, **27**: 1565 (2007); https://doi.org/10.1016/j.jeurceramsoc.2006.04.121
18. A.R. Studart, F. Filser, P. Kocher, and L.J. Gauckler, *Biomaterials*, **28**: 2695 (2007); https://doi.org/10.1016/j.biomaterials.2006.12.033
19. A.J. Raigrodski, *J. Prosthet. Den.*, **92**: 557 (2004); https://doi.org/10.1016/j.prosdent.2004.09.015
20. I. Denry, J.R. Kelly, *Dent. Mater.*, **24**: 299 (2008); https://doi.org/10.1016/j.dental.2007.05.007
21. S. Saridag, O. Tak, and G. Alniacik, *World J. Stomatology*, **2**: 40 (2013); https://doi.org/10.5321/wjs.v2.i3.40
22. R.C. Garvie, R.H. J. Hannink, and R.T. Pascoe, *Nature*, **258**: 703 (1975); https://doi.org/10.1038/258703a0
23. Richard H.J. Hannink, Patrick M. Kelly, and Barry C. Muddle, *J. Am. Ceram. Soc.*, **83**: 461 (2000); https://doi.org/10.1111/j.1151-2916.2000.tb01221.x
24. Vinciane Koenig, Claudine P. Wulfman, Mathieu A. Derbanne, Nathalie M. Dupont, Stephane O. Le Goff, Mie-Leng Tang, Laurence Seidel, Thibaut Y. Dewael, Alain J. Vanheusden, and Amelie K. Mainjot, *Contemporary Clinical Trials Communications*, **4**: 25 (2016); https://doi.org/10.1016/j.conctc.2016.06.001
25. Claudia Bngela Maziero Volpato, Luis Gustavo D'Altoe Garbelotto, Marcio Celso Fredel, and Federica Bondioli, Application of zirconia in dentistry: biological, mechanical and optical considerations, *Advances in Ceramics: Electric and Magnetic Ceramics, Bioceramics, Ceramics* (Croatia: InTech: 2011); https://doi.org/10.5772/21630
26. R.C. Garvie and P.S. Nicholson., *J. American Ceramic Society,* **55**: 152 (1972); https://doi.org/10.1111/j.1151-2916.1972.tb11290.x
27. C. Piconi and G. Maccauro, *Biomaterial*s, **20**: 1 (1999); https://doi.org/10.1016/S0142-9612(98)00010-6
28. A.H. Heuer, F.F. Lange, Swain M.V., and A.G. Evans, *J. Am. Ceram. Soc.,* **69**: 1 (1986);

https://doi.org/10.1111/j.1151-2916.1986.tb07400.x
29. N.R. Silva, L. Witek, P.G. Coelho, V.P. Thompson, E.D. Rekow, and J. Smay, *J. Prosthodont.*, **20**: 93 (2011);
https://doi.org/10.1111/j.1532-849X.2010.00623.x
30. J.R. Strub, E.D. Rekow, and S. Witkowski, *J. Am. Dent. Assoc.*, **137**: 1289 (2006);
https://doi.org/10.14219/jada.archive.2006.0389
31. V. Preis, M. Behr , S. Hahnel, G. Handel, and M. Rosentritt, *J. Dent.*, **40**: 921 (2012);
https://doi.org/10.1016/j.jdent.2012.07.010
32. A. Afzal, *Materials Express*, **4**: 1 (2014);
https://doi.org/10.1166/mex.2014.1148
33. A. Azari, and S. Nikzad, *Rapid Prototyping Journal*, **15**: 216 (2009);
https://doi.org/10.1108/13552540910961946
34. Z.C. Eckel, C. Zhou, J.H.Martin, A.J. Jacobsen, W.B. Carter, and T.A. Schaedler, *Science*, **351**: 58 (2016);
https://doi.org/10.1126/science.aad268
35. M.L. Griffith and J.W. Halloran, *J. Am. Ceram. Soc.*, **79**: 2601 (1996);
https://doi.org/10.1111/j.1151-2916.1996.tb09022.x
36. J.C. Wang, and H. Dommati, *Int. J. Adv. Manu.f Technol.*, **98**: 1537 (2018);
https://doi.org/10.1007/s00170-018-2349-3
37. S.H. Suleiman and Vult von Steyern P., *Acta Odontol. Scand.*, **71**:1280 (2013);
https://doi.org/10.3109/00016357.2012.757650
38. E.J. Bae, Jeong I.D., Kim W.C., Kim J.H., *J. Prosthet. Dent.*, **118**: 187 **(**2017);
https://doi.org/10.1016/j.prosdent.2016.11.004
39. M Ozcan, *J. Oral Rehabilitation*, **30**: 265 (2003);
https://doi.org/10.1046/j.1365-2842.2003.01038.x
40. D.A. Oram and E.H. Cruickshank-Boyd, *J. Prosthetic Dentistry*, **52**: 221 (1984);
https://doi.org/10.1016/0022-3913(84)90100-8
41. A. Eliasson, C.F. Arnelund, and A. Johansson, *J. Prosthet. Dent.*, **98**: 6 (2007);
https://doi.org/10.1016/S0022-3913(07)60032-8
42. T.B.W. Marchack, L.B. Chen, C.B. Marchack, and Y. Futatsuki, *The J. Prosthetic Dentistry*, **98**: 478 (2007);
https://doi.org/10.1016/s0022-3913(07)60148-6
43. C. Gautam, J. Joyner, A. Gautam, J. Rao, and R. Vajtai, *Dalton Transactions*, **45**:19194 (2016);
https://doi.org/10.1039/C6DT03484E
44. M. Guazzato, M.A lbakry, S.P. Ringer, and M.V. Swain, *Dental Mater.*, **20**: 449 (2004);
https://doi.org/10.1016/j.dental.2003.05.002
45. S.D. Heintze and V. Rousson, *The Int. J. Prosthodontics*, 2010; **23**: 493 (2010);
https://doi.org/10.1155/2015/392496
46. Ginny Soon, Belinda Pingguan-Murphy, Khin WeeLai, and Sheikh Ali Akbar, *Ceramics Int.*, **42**: 12543 (2016);
https://doi.org/10.1016/j.ceramint.2016.05.077
47. Brian R. Stoner, Jason A. Griggs, John Neidigh, and Jeffrey R. Piascik, *J. Biomedical Mater. Res.*, **102**: 441 (2014);
https://doi.org/10.1002/jbm.b.33021
48. Shyh-Yuan Lee, and Cho-Pei Jiang, *Mater. Manufacturing Proc.*, **30**: 1498 (2015);
https://doi.org/10.1080/10426914.2014.984208

49. J. Chevalier, S. Deville, E. Munch, R. Jullian, and F. Lair, *Biomaterials*, **25**: 5539 (2004); https://doi.org/10.1016/j.biomaterials.2004.01.002
50. J.P. Goff, W. Hayes, S. Hull, M.T. Hutchings, and K.N. Clausen, *Phys. Rev. B: Cond. Matter.*, **59**, No. 22: 14202 (1999); https://doi.org/10.1103/PhysRevB.59.14202
51. K. Kobayashi, H. Kuwajima, and T. Masaki, *Solid State Ionics*, **3–4**: 489 (1981); https://doi.org/10.1016/0167-2738(81)90138-7
52. A.E. Rodriguez, M. Monzavi, C.L. Yokoyama, and H. Nowzari, *J. Esthet. Restor. Dent.*, **30**: 538 (2018); https://doi.org/10.1111/jerd.12414
53. R.B. Osman and M.V. Swain, *Materials,* **8**: 932 (2015); https://doi.org/10.3390/ma8030932
54. H. Nakai, M. Inokoshi, K. Nozaki, K. Komatsu, S. Kamijo, H. Liu, M. Shimizubata, S. Minakuchi B. Van Meerbeek, J. Vleugels, and F. Zhang, *Materials*, **14**: 3694 (2021); https://doi.org/10.3390/ma14133694
55. Khuram Shahzad, Jan Deckers, Zhongying Zhang, Jean-Pierre Kruth, and Jef Vleugels, *J. Eur. Ceram. Soc.*, **34**: 81 (2014); https://doi.org/10.1016/j.jeurceramsoc.2013.07.023
56. A.C. Branco, R. Silva, T. Santos, H. Jorge, A.R. Rodrigues, R. Fernandes, S. Bandarra, I. Barahona, A.P.A. Matos, K. Lorenz, M. Polido, R. Colaço, A.P. Serro, and C.G. Figueiredo-Pina, *Dent. Mater.*, **36**: 442 (2020); https://doi.org/10.1016/j.dental.2020.01.006
57. L.N. Khanlar, A. Salazar Rios, A. Tahmaseb, and A. Zandinejad, *Dent. J.*, **9**: 104 (2021); https://doi.org/10.3390/dj9090104
58. C. Hull, *Apparatus for Production of Three-Dimensional Objects by Stereolithography* (U.S. Patent No. 4575 330: 1986).
59. Lian Qin, Wenquan Sui, Xiangquan Wu, Fei Yang, and Shaopeng Yang, *Rapid Prototyping J.*, **24**: 114 (2018); https://doi.org/10.1108/RPJ-09-2016-0144
60. V. Tomeckova, J.W. Halloran, *J. Eur. Ceram. Soc.*, **30**: 3273 (2010); https://doi.org/10.1016/j.jeurceramsoc.2010.08.003
61. W. Huang, X. Kang, C. Xu, J. Zhou, J. Deng, Y. Li, and S. Cheng, *Adv. Mater.*, **30**: 1706962 (2018); https://doi.org/10.1002/adma.201706962
62. Y. Zeng, Y.Z. Yan, H.F. Yan, C.C. Liu, P.R. Li, P. Dong, Y. Zhao, and J.M. Chen, *J. Mater. Sci.*, **53**: 6291 (2018); https://doi.org/10.1007/s10853-018-1992-2
63. J. Guo, Y. Zeng, P.R. Li, and J.M. Chen, *Ceram. Int.*, **17**: 23007 (2019); https://doi.org/10.1016/j.ceramint.2019.07.346
64. X.A. Shuai, Y. Zeng, P.R. Li, and J.M. Chen, *J. Mater. Sci.*, **55**: 6771 (2020); https://doi.org/10.1007/s10853-020-04503-y
65. Gerald Mitteramskogler, Robert Gmeiner, Ruth Felzmann, Simon Gruber, Christoph Hofstetter, Jurgen Stampfl, Jorg Ebert, Wolfgang Wachter, and Jorgen Laubersheimer, *Additive Manufacturing*, **1–4**: 110 (2014); https://doi.org/10.1016/j.addma.2014.08.003
66. Haoyuan Quan, Ting Zhang, Hang Xu, Shen Luo, Jun Nie, and Xiaoqun Zhu, *Bioact. Mater.*, **5**: 110 (2020);

https://doi.org/10.1016/j.bioactmat.2019.12.003
67. L.J. Hornbeck, *Frame Addressed Spatial Light Modulator* (U.S. Patent 4615595 (1986).
68. Z. Zhao, X. Tian, and X. Song, *J. Mater. Chem. C*, **8**: 11561 (2020); https://doi.org/10.1039/D0TC03548C
69. Jiumeng Zhang, Qipeng Hu, Shuai Wang, Jie Tao, and Maling Go, *Int. J. Bioprint.*, **6**, No. 1: 242 (2020); https://doi.org/10.18063/ijb.v6i1.24270
70. Emre Ozkol, Wen Zhang, Jorg Ebert, and Rainer Telle, *Journal of the European Ceramic Society*, **32**: 2193 (2012); https://dx.doi.org/10.1016/j.jeurceramsoc.2012.03.006
71. Bartolomeo Coppola, Nicola Cappetti, Luciano Di Maio, Paola Scarfatoand, and Loredana Incarnato, *Materials*, **11**: 1947 (2018); https://doi.org/10.3390/ma11101947
72. Qin Lian, Wenquan Sui, Xiangquan Wu, Fei Yang, and Shaopeng Yang, *Rapid Prototyping J.*, **24**: 114 (2018); https://doi.org/10.1108/RPJ-09-2016-0144
73. Jussi M. Suominen, Erkka J. Frankberg, Pekka K. Vallittu, Erkki Levdnen, Jorma Vihinen, Teemu Vastamdki, Risto Kari and Lippo V.J. Lassila, *Biomaterial Investigations in Dentistry*, **6**: 23 (2019); https://doi.org/10.1080/26415275.2019.1640608
74. Hiroto Nakai, Masanao Inokoshi, Kosuke Nozaki, Keiji Komatsu, Shingo Kamijo, Hengyi Liu, Makoto Shimizubata, Shunsuke Minakuchi, Bart Van Meerbeek, Jef Vleugels, and Fei Zhang, *Materials,* **14***:* 3694 (2021); https://doi.org/10.3390/ma14133694
75. Reham B. Osman, Albert J. van der Veen, Dennis Huiberts, Daniel Wismeijer, and Nawal Alhar, *J. Mechanical Behavior of Biomedical Materials*, **75**: 521 (2017); https://doi.org/10.1016/j.jmbbm.2017.08.018
76. Hezhen Li, Lu Song, Jialin Sun, Jing Ma, and Zhijian Shen, *Adv. Appl. Ceram.*, **118**: 30 (2019); https://dx.doi.org/10.1080/17436753.2018.1447834
77. Kyoung-Jun Jang, Jin-Ho Kanga, John G. Fisher, and Sang-Won Park, *Dental Mater.*, **35**, No. 5: e97 (2019); https://doi.org/10.1016/j.dental.2019.02.001
78. Ziyu Mei, Yuqing Lu, Yuxin Lou, Ping Yu, Manlin Sun, Xin Tan, Junjing Zhang, Li Yue, and Haiyang Yu, *BioMed Res. Int.*, **2021**: 6612840; https://doi.org/10.1155/2021/6612840
79. Bartolomeo Coppola, Julien Schmitt, Tanguy Lacondemine, Caroline Tardivat, Laura Montanaro, and Paola Palmero, *J. Eur. Ceram. Soc.*, **42**: 2974 (2022); https://doi.org/10.1016/j.jeurceramsoc.2022.01.024
80. Reem Abualsaud, Maissan Abussaud, Yara Assudmi, Ghadah Aljoaib, Abrar Khaled, Haidar Alalawi, Sultan Akhtar, Asif Matin, and Mohammed M. Gad, *Materials*, **15**: 6988 (2022); https://doi.org/10.3390/ma15196988

Received 28.01.2023;
in final version, 01.02.2023

М.О. Васильєв[1], *П.О. Гурин*[2]

[1] Інститут металофізики ім. Г.В. Курдюмова НАН України,
бульв. Акад. Вернадського, 36, 03142 Київ, Україна

[2] Національний університет охорони здоров'я України імені П.Л. Шупика,
вул. Дорогожицька, 9, 04112 Київ, Україна

СТРУКТУРА ТА ВЛАСТИВОСТІ НАДРУКОВАНОГО НА 3*D*-ПРИНТЕРІ ДІОКСИДУ ЦИРКОНІЮ, ВИКОРИСТОВУВАНОГО В СТОМАТОЛОГІЇ

Останніми роками інтерес до застосування адитивного виробництва (АВ), також відомого як 3*D*-друк, стає надзвичайно популярним у різних галузях медицини, включаючи стоматологію. В даний час для протезування зубів, виготовлених методом 3*D*-друку, найчастіше використовуються металеві та керамічні матеріали. Кераміка з діоксиду Цирконію, стабілізована оксидом Ітрію (YSZ), стала найліпшою альтернативою для реставрації зубів на металевій основі. У зв'язку з цим основна мета цього огляду полягає у вивченні впливу параметрів 3*D*-друку на макро- та мікроструктуру і, відповідно, на механічні властивості спеченого діоксиду Цирконію YSZ, а на основі цього надати практичні рекомендації для клінічної стоматології та подальші перспективи. Найбільш дослідженими за останні роки методами 3*D*-друку такої кераміки є лазерна стереолітографія (Laser-SL) і стереолітографічне цифрове оброблення світлом (SL-DLP), засновані на технології фотополімеризації у ванні. Розглянуто фізичні основи та технологічні параметри цих АВ-технологій. Основну увагу зосереджено на впливі теплових умов під час 3*D*-друку на мікроструктуру затвердіння (щільність, розмір зерна та кристалічний фазовий склад), яка контролюється технологіями виробництва. Також обговорюється справжня твердість і двовісна міцність на вигин зразків YSZ, надрукованих на 3*D*-принтері. Нарешті згадуються переваги 3*D*-друку кераміки в стоматології.

Ключові слова: стоматологія, адитивне виробництво, 3*D*-друк, діоксид Цирконію, мікроструктура, твердість, міцність на згин.